JACS
JOURNAL OF THE AMERICAN CHEMICAL SOCIETY
pubs.acs.org/JACS
Article

Laser-Triggered Bottom-Up Transcription of Chemical Information: Toward Patterned Graphene/MoS_2 Heterostructures

Xin Chen, Mhamed Assebban, Malte Kohring, Lipiao Bao, Heiko B. Weber, Kathrin C. Knirsch, and Andreas Hirsch*

Cite This: J. Am. Chem. Soc. 2022, 144, 9645−9650
Read Online
ACCESS | Metrics & More | Article Recommendations | Supporting Information

ABSTRACT: Efficiently assembling heterostructures with desired interface properties, stability, and facile patternability is challenging yet crucial to modern device fabrication. Here, we demonstrate an interface coupling concept to bottom-up construct covalently linked graphene/MoS_2 heterostructures in a spatially defined manner. The covalent heterostructure domains are selectively created in analogy to the traditional printmaking technique, enabling graphic patterns at the bottom MoS_2 layer to be precisely transferred to the top graphene layer. This bottom-up connection and transcription of chemical information is achieved simply via laser beam irradiation. Our approach opens up a new paradigm for heterostructure construction and integration. It enables the efficient generation and real-time visualization of spatially well-resolved covalent graphene/MoS_2 heterostructures, facilitating further design and integration of patterned heterostructures into new generations of high-performance devices.

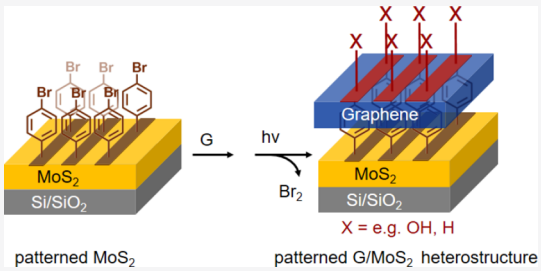

INTRODUCTION

The emerging field of two-dimensional (2D) materials has led to the isolation and characterization of a large variety of 2D crystals with fascinating properties.[1−4] The fabrication of heterostructures by combining these 2D crystals into one vertical stack has evolved as an appealing strategy to increase structural and functional complexity. On the one hand, it enables synergetic effects of different components, and on the other hand, it provides a way to overcome the limitations of individual materials.[5,6] Among the heterostructures investigated so far, graphene/MoS_2 (G/MoS_2) sandwiches have drawn particular attention due to their extraordinary properties and great potential in high-performance devices such as electronic,[7−9] optoelectronic,[10,11] energy storage,[12,13] and neuromorphic devices,[14] gas and biosensors,[15,16] and catalysts.[17] Direct stacking of dangling-bond-free 2D nanosheets to form purely van der Waals (vdW) heterostructures with atomically clean interfaces has been actively pursued in recent years.[5,18,19] However, for most vdW interfaces, the structural disorders and contaminations induced by the integration steps impose serious technical challenges to the interface quality that could severely limit the electronic communication and the device efficacy.[20] In addition, the stability and reliability of heterostructures remain challenging tasks.[18,19] To achieve efficient interface charge transport and chemical robustness, assembling of covalently linked G/MoS_2 heterostructures represents a viable approach being still largely unexplored.[21,22] In particular, no direct linking of intact graphene nanosheets with high-quality MoS_2 single layers has been accomplished so far.

Here, we report for the first time an efficient and facile approach to fabricate covalently linked G/MoS_2 heterostructures directly on a silicon substrate. Covalent binding of pristine graphene nanosheets to monolayer MoS_2 nanosheets was achieved simply through a laser-triggered interface coupling reaction, greatly saving the processing time. Furthermore, with patterned MoS_2 as the bottom layer, we were able to generate patterned G/MoS_2 heterostructures with both vdW and covalent heterostructure domains by laser irradiation, which enables an efficient, controllable, and regioselective fabrication of heterostructures. The formation of these patterned heterostructures was demonstrated by Raman, photoluminescence (PL), and Kelvin probe force microscopy (KPFM) mappings, which allows us to identify the boundaries and the distinct characteristics of vdW and covalent heterostructures. Our approach enables the high throughput generation of covalent heterointerfaces and precise transcription of spatial patterns from the bottom to the top layer of the heterostructures. This paves the way for further

Received: January 18, 2022
Published: May 26, 2022

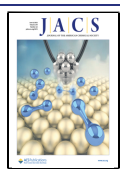

https://doi.org/10.1021/jacs.2c00642
J. Am. Chem. Soc. 2022, 144, 9645−9650

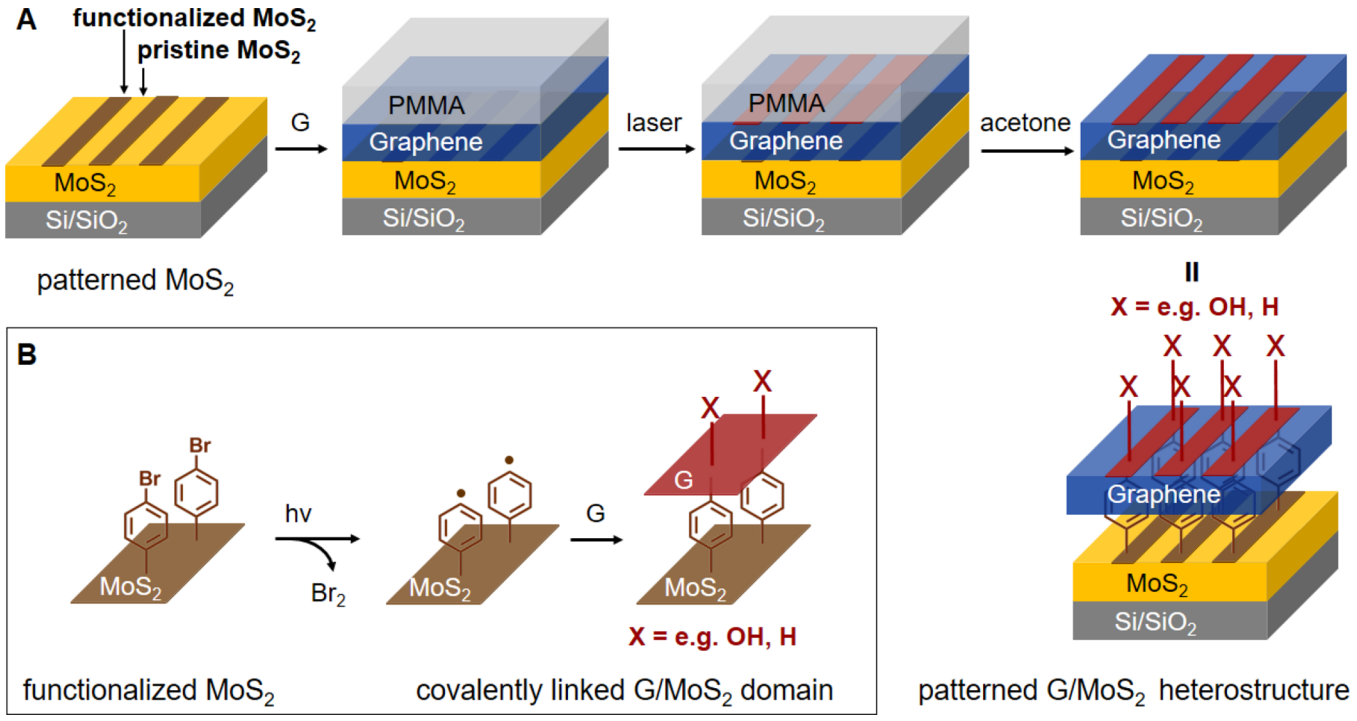

Figure 1. (A) Schematic illustration of the fabrication process for the patterned G/MoS_2 heterostructures. The brown stripes in the patterned MoS_2 indicate the functionalized MoS_2 regions. The red stripes in the patterned G/MoS_2 heterostructures indicate the covalent heterostructure domains, which are formed exclusively between functionalized MoS_2 and graphene. (B) Graphic illustration of the formation of a G/MoS_2 covalent domain through a laser-triggered interface coupling reaction. It involves two major steps: (i) Laser photon-initiated debromination and phenyl radical formation and (ii) functionalization of the bottom side of graphene with local phenyl radicals. The built-up strain on graphene caused by the interface coupling is likely relieved through the antaratopic additions of H or OH groups to the top side of graphene.[25]

integration of fabricated heterostructures into highly integrated devices.

RESULTS AND DISCUSSION

Figure 1A depicts the fabrication steps of the bottom-up assembly of patterned G/MoS_2 heterostructures. We started with patterned CVD MoS_2[23] as the bottom layer previously developed in our group. Subsequently, a CVD graphene film covered with a polymethylmethacrylate (PMMA) layer was vertically placed on the top of the patterned MoS_2 surface. This vertical stack was then subjected to Raman laser irradiation. After removal of the PMMA mask, the patterned G/MoS_2 heterostructures were formed. On the patterned MoS_2 surface, the functionalized MoS_2 stripes (brown regions, width = 4 μm) and pristine MoS_2 gaps (width = 8 μm) are alternately distributed. Under laser irradiation, the covalently tethered 4-bromophenyl groups in the functionalized MoS_2 region eliminate bromine radicals leaving behind highly reactive phenyl radicals.[24] The phenyl radicals then attack the graphene lattice from underneath to form the patterned and covalently linked heterostructures (Figure 1B). The interface coupling solely takes place between the covalently functionalized MoS_2 regions and the top layer graphene nanosheet allowing for spatially controlled covalent transcription. The remaining unfunctionalized regions of pristine graphene and pristine MoS_2 form patterned vdW domains.

The Raman spectra (Figure 2) of both vdW and covalent heterostructure domains display the characteristic peaks from both MoS_2 (E^1_{2g} and A_{1g} modes) and graphene (G and 2D bands). The Raman spectrum of vdW domains exhibits a negligible D band, a slightly increased bandwidth of the G band, and the similar bandwidth of the 2D band to pristine graphene, suggesting that the laser irradiation and the vertical stacking of graphene onto the top of the MoS_2 layer did not cause significant defects. Compared to vdW domains, the Raman spectrum of covalent domains shows a prominent D

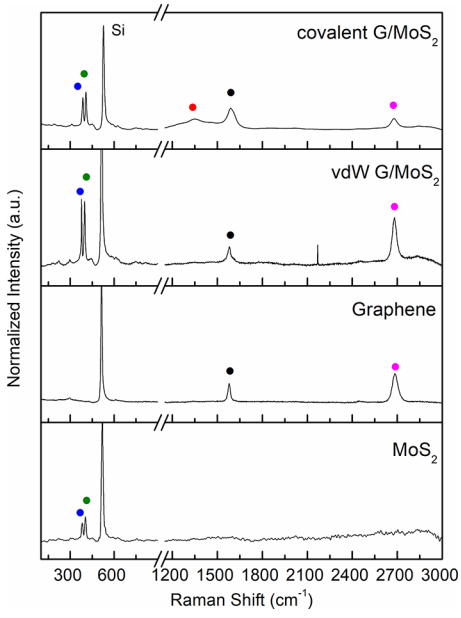

Figure 2. Raman spectra (λ = 532 nm) of MoS_2, graphene, vdW G/MoS_2 heterostructures, and covalent G/MoS_2 heterostructures. The color code for the Raman peaks: E^1_{2g} mode (blue), A_{1g} mode (green), G band (black), D band (red), and 2D band (pink).

https://doi.org/10.1021/jacs.2c00642
J. Am. Chem. Soc. 2022, 144, 9645−9650

band, a smaller 2D band, as well as a broader G mode (Table S1), suggesting the presence of defects in the graphene layer of the covalent domain. These defects were introduced through the laser-triggered covalent functionalization, forming the covalent bonds at the interface and the surface.[26,27] In addition, a close look at the low-frequency region of the Raman spectra (Figure S1) revealed a downshifted peak position and a broadened peak width of Raman A_{1g} mode in covalent domains compared to vdW domains, indicating that the MoS_2 layer at the covalent domain was n-doped,[28] possibly through the covalent interface coupling.

The distinct and characteristic Raman features of vdW and covalent domains allow us to estimate the efficiency of covalent interface generation by analyzing the defect density within the graphene layers. To this end, we monitored the Raman evolution (Figures S2 and S4) of both vdW and covalent heterostructure domains as a function of the irradiation conditions (laser power and irradiation time) and evaluated the defect density within the graphene layer in each case by plotting the peak intensity ratio of D to G bands, denoted as $I(D)/I(G)$, against the irradiation conditions (Figures S3 and S5). At the same irradiation time but increased laser power, there was only a slight increase of the D band intensity for the vdW domains (Figure S2A), indicating that laser irradiation can only induce negligible defects at the pristine graphene/MoS_2 stack. In comparison, the intensity of the D band of the covalent domains is significantly increased (Figure S2B), suggesting that the formation of defects at covalent domains is highly dependent on the laser power. As the number of bromophenyl groups, determined by the degree of covalent functionalization of MoS_2, is fixed, the laser power-dependent feature of this covalent interaction at the interface indicates that the rate-limiting step is laser-triggered, most likely is the photon-induced debromination. Therefore, the actual active moieties are the available phenyl radicals as we depicted in Figure 1B. The more energy was employed, the more phenyl radicals were generated, and the more sp^3-hybridized C-atoms (defects) in graphene would form through the covalent bonding to phenyl radicals. Indeed, the plots of $I(D)/I(G)$ vs laser power (Figure S3, dark trace) show a marginal change within the vdW domains with the value of $I(D)/I(G)$ ranging between 0.1 and 0.2. On the other hand, the covalent domains (Figure S3, red trace) show a monotonic growth of $I(D)/I(G)$ with increasing laser power. The maximum value of $I(D)/I(G)$ is about 0.7, implying that the graphene layer at the covalent domain can be highly functionalized when employing high laser power irradiation.

Similarly, Raman measurements under the same laser power but at extended irradiation times were also performed to vdW and covalent domains. The Raman spectra (Figure S4) of both vdW and covalent domains showed little changes only with an $I(D)/I(G)$ value of about 0.29 ± 0.06 for vdW domains and 0.54 ± 0.02 for covalent domains (Figure S5). The value of $I(D)/I(G)$ indicates that the defect density was retained at a similar level over these extended irradiation times. For the covalent domain, this phenomenon can be ascribed to fast radical reaction kinetics. The covalent interface coupling reaction was completed within 10 s. Therefore, the degree of functionalization (or defect density) has likely reached the maximum before the chosen time.

Having figured out that relatively high laser power favors the interface coupling, we introduced a writing-reading cycle for the high-contrast Raman spatial mapping. In the first scan, a high laser power was employed to only irradiate the area consisting of the pristine graphene and the functionalized MoS_2 (writing process). This writing process allows the efficient generation of a covalent interface. In the second scan, a low laser power was used to scan through the entire patterned area (reading process). The Raman spatial maps obtained from the reading process are shown in Figure 3. The

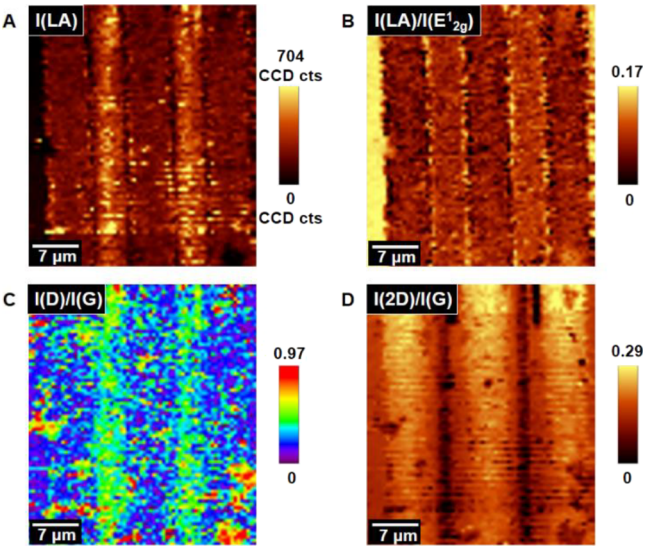

Figure 3. Raman spatial maps (λ = 532 nm) of the patterned G/MoS_2 heterostructure obtained from the reading process. (A) Raman map of the intensity of LA mode. (B) Raman map of the intensity ratio of LA to E^1_{2g} mode. (C) Raman map of the intensity ratio of D to G bands. The full color scale was chosen for easy recognition. (D) Raman map of the intensity ratio of 2D to G bands. The covalent heterostructure domains are the areas with the higher I(LA), higher $I(LA)/I(E^1_{2g})$, higher $I(D)/I(G)$, but lower $I(2D)/I(G)$.

regions containing functionalized MoS_2 can be identified as the bright stripes with increased intensities of the LA mode (Figure 3A) and increased intensity ratios of the LA to E^1_{2g} modes (LA/E^1_{2g}, Figure 3B).[29,30] The regions containing functionalized graphene are recognized as the thinner stripes with the higher $I(D)/I(G)$ (Figure 3C) and lower $I(2D)/I(G)$ ratios (Figure 3D). Most importantly, the location of functionalized graphene stripes correlates very well with that of functionalized MoS_2 stripes, suggesting the successful generation of covalently linked G/MoS_2 heterostructure domains on the top of functionalized MoS_2 regions. Remarkably, it demonstrates the possibility to transcribe the topographic pattern and chemical information through the covalent linkages at the heterointerface. Moreover, the boundaries and optical characteristics of vdW and covalent heterostructure domains, which are difficult to determine from the optical images (Figure S6), can be easily distinguished from these Raman maps, providing a convenient tool to track and compare the heterointerface formation.

We also screened other irradiation conditions (Figure S7). It is possible to generate and visualize the covalent domains in one irradiation cycle; however, the boundaries between vdW and covalent domains are less resolved compared to that obtained from the writing-reading cycle. By adopting this laser-writing-facilitated bottom-up assembly strategy, we managed to create other more delicate patterned heterostructures such as

https://doi.org/10.1021/jacs.2c00642
J. Am. Chem. Soc. 2022, 144, 9645−9650

the FAU logo and dot arrays with a minimum feature size of 2 μm (Figure S8).

The distinct surface characteristics of vdW and covalent heterostructures are also reflected by the PL measurements. Compared to the vdW domains, the covalent domains show remarkably decreased intensities of the A exciton (Figure 4A),

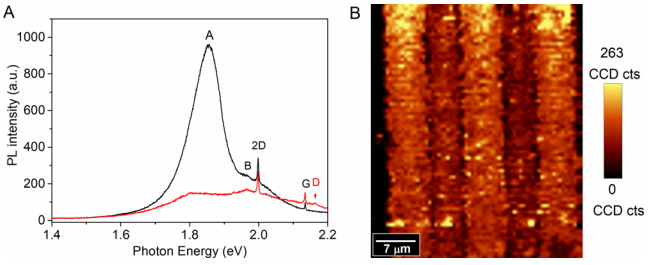

Figure 4. (A) PL spectra (λ = 532 nm) of vdW (black) and covalent (red) G/MoS_2 domains. (B) PL intensity map of the A exciton for the patterned G/MoS_2 heterostructure. The covalent domains are shown as the darker stripes with the lower PL intensities of the A exciton.

which is likely due to the efficient charge transfer at the covalently bonded interface. The PL map of the A exciton intensities (Figure 4B) displays switchable photoluminescence: the vdW domains feature the bright regions (switch-on) with higher PL intensities of the A exciton, whereas the covalent ones feature the darker stripes (switch-off) with lower PL intensities of the A exciton. This experiment demonstrates the possibility of switching the photoluminescence of heterostructures by selective manipulation of the bonding state at the heterointerface, which is of great importance for future optoelectronic device fabrication.

Further characterization using KPFM (Figure 5A) shows an alternately distributed stripe pattern, suggesting a clear surface

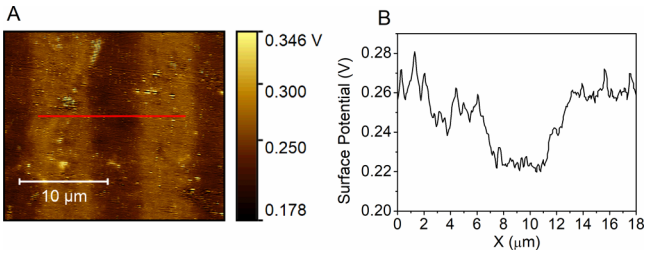

Figure 5. (A) KPFM image of patterned G/MoS_2 heterostructures. (B) Surface potential measured along the red line shown in (A).

potential variation between vdW and covalent heterostructure domains. Compared to the vdW domains, the surface potential of the covalent domain dropped by 0.04 V (Figure 5B), indicating that the work function of the covalent heterostructure is slightly increased. This phenomenon was likely attributed to an interface covalent bonding-induced doping effect.[31,32]

To elucidate the role of substituents in the covalent coupling reaction, we also investigated blind experiments using presumably inert substituents (e.g., 4-nitrophenyl and 4-methoxyphenyl) on the MoS_2 surface and pristine CVD MoS_2. However, none of these stacked structures showed the D band intensity enhancement in Raman spectra (Figure S9), suggesting that graphene was not functionalized in these cases.

As we stated in the beginning, the interface coupling of graphene to MoS_2 involves light-triggered radical formations followed by subsequent radical attacks to graphene. To further verify the probability of functionalization of graphene via the radical attacks, initiated by Br elimination of phenyl- or benzyl bromides, two control experiments were performed. In the first experiment (Figure S10A), bromobenzene (BB) was drop-cast on a clean surface of a silicon wafer, then monolayer graphene was placed on top. The sample was then subjected to laser irradiation. With increasing the laser intensity, the Raman spectra (Figure S10B) of G/BB display significantly increased D band and reduced 2D band intensities, suggesting that the graphene layer in G/BB was successfully functionalized. In the second experiment, the self-assembled (SAM) layer of 4-bromobenzylphosphonic acid was initially anchored on the surface of the silicon wafer.[33] Then, graphene was transferred to the top of the SAM layer (Figure S11A). The sample was then subjected to Raman laser irradiation. Again, the growth of the D band intensities and the decrease in the 2D band intensities were observed with an increase in laser power (Figure S11B). This again is a clear indication of a very efficient covalent graphene functionalization. These two reference experiments further confirm that light-induced radical formation out of organobromides is a selective method for patterning transcription and the formation of covalent heterostructures.

CONCLUSIONS

In summary, we have demonstrated that laser-triggered covalent interface formation is an effective approach to integrate G/MoS_2 heterostructures featuring efficient charge transport and facile patternability. The organic linkers at the interface are the pillars of the covalent assembly, allowing for leveraging the optical and electronic responses with molecular engineering. By employing laser-writing techniques and prepatterned MoS_2 as the bottom layer, the covalent G/MoS_2 heterostructures can be selectively generated, forming a patterned heterostructure surface that copies from the bottom template. Our approach enables simultaneous covalent interface formation and topographic pattern transcription, facilitating the mass production of heterostructures. This covalent assembly concept has great potential to be extended to the construction of a broad array of two-layer or multilayered covalent heterostructures, which is pivotal for future material design and engineering.

ASSOCIATED CONTENT

Supporting Information

The Supporting Information is available free of charge at https://pubs.acs.org/doi/10.1021/jacs.2c00642.

General information about materials, experimental procedures, characterization, and instrumentation; experimental details for doping effects on MoS_2 Raman scattering; screening of irradiation conditions; Raman spatial maps obtained from the one-scanning process; Raman spatial maps for other patterned heterostructures; and reference experiments (PDF)

AUTHOR INFORMATION

Corresponding Author

Andreas Hirsch − *Department of Chemistry and Pharmacy, Friedrich-Alexander-Universität Erlangen-Nürnberg (FAU), Erlangen 91058, Germany;* orcid.org/0000-0003-1458-8872; Email: andreas.hirsch@fau.de

https://doi.org/10.1021/jacs.2c00642
J. Am. Chem. Soc. 2022, 144, 9645−9650

Authors

Xin Chen − *Department of Chemistry and Pharmacy, Friedrich-Alexander-Universität Erlangen-Nürnberg (FAU), Erlangen 91058, Germany*

Mhamed Assebban − *Department of Chemistry and Pharmacy, Friedrich-Alexander-Universität Erlangen-Nürnberg (FAU), Erlangen 91058, Germany*

Malte Kohring − *Department of Physics, Friedrich-Alexander-Universität Erlangen-Nürnberg (FAU), Erlangen 91058, Germany*

Lipiao Bao − *Department of Chemistry and Pharmacy, Friedrich-Alexander-Universität Erlangen-Nürnberg (FAU), Erlangen 91058, Germany;* orcid.org/0000-0002-6308-1181

Heiko B. Weber − *Department of Physics, Friedrich-Alexander-Universität Erlangen-Nürnberg (FAU), Erlangen 91058, Germany;* orcid.org/0000-0002-6403-9022

Kathrin C. Knirsch − *Department of Chemistry and Pharmacy, Friedrich-Alexander-Universität Erlangen-Nürnberg (FAU), Erlangen 91058, Germany*

Complete contact information is available at: https://pubs.acs.org/10.1021/jacs.2c00642

Notes

The authors declare no competing financial interest.

■ ACKNOWLEDGMENTS

This project has received funding from the European Union's Horizon 2020 research and innovation programme Graphene Flagship under grant agreement No 881603 and the Deutsche Forschungsgemeinschaft (DFG, German Research Foundation), Projektnummer 182849149-SFB 953 "Synthetic Carbon Allotropes"- A1 and B8.

■ REFERENCES

(1) Tan, C.; Cao, X.; Wu, X.-J.; He, Q.; Yang, J.; Zhang, X.; Chen, J.; Zhao, W.; Han, S.; Nam, G.-H.; Sindoro, M.; Zhang, H. Recent Advances in Ultrathin Two-Dimensional Nanomaterials. *Chem. Rev.* **2017**, *117*, 6225−6331.

(2) Chhowalla, M.; Shin, H. S.; Eda, G.; Li, L.-J.; Loh, K. P.; Zhang, H. The chemistry of two-dimensional layered transition metal dichalcogenide nanosheets. *Nat. Chem.* **2013**, *5*, 263−275.

(3) Pumera, M.; Sofer, Z. 2D Monoelemental Arsenene, Antimonene, and Bismuthene: Beyond Black Phosphorus. *Adv. Mater.* **2017**, *29*, No. 1605299.

(4) Khan, K.; Tareen, A. K.; Aslam, M.; Wang, R.; Zhang, Y.; Mahmood, A.; Ouyang, Z.; Zhang, H.; Guo, Z. Recent developments in emerging two-dimensional materials and their applications. *J. Mater. Chem. C* **2020**, *8*, 387−440.

(5) Novoselov, K. S.; Mishchenko, A.; Carvalho, A.; Castro Neto, A. H. 2D materials and van der Waals heterostructures. *Science* **2016**, *353*, No. aac9439.

(6) Wang, S.; Cui, X.; Jian, C. E.; Cheng, H.; Niu, M.; Yu, J.; Yan, J.; Huang, W. Stacking-Engineered Heterostructures in Transition Metal Dichalcogenides. *Adv. Mater.* **2021**, *33*, No. 2005735.

(7) Shih, C.-J.; Wang, Q. H.; Son, Y.; Jin, Z.; Blankschtein, D.; Strano, M. S. Tuning On−Off Current Ratio and Field-Effect Mobility in a MoS_2−Graphene Heterostructure via Schottky Barrier Modulation. *ACS Nano* **2014**, *8*, 5790−5798.

(8) Tang, Z.; Liu, C.; Huang, X.; Zeng, S.; Liu, L.; Li, J.; Jiang, Y.-G.; Zhang, D. W.; Zhou, P. A Steep-Slope MoS_2/Graphene Dirac-Source Field-Effect Transistor with a Large Drive Current. *Nano Lett.* **2021**, *21*, 1758−1764.

(9) Lee, E.; Lee, S. G.; Lee, W. H.; Lee, H. C.; Nguyen, N. N.; Yoo, M. S.; Cho, K. Direct CVD Growth of a Graphene/MoS_2 Heterostructure with Interfacial Bonding for Two-Dimensional Electronics. *Chem. Mater.* **2020**, *32*, 4544−4552.

(10) Zhang, W.; Chuu, C.-P.; Huang, J.-K.; Chen, C.-H.; Tsai, M.-L.; Chang, Y.-H.; Liang, C.-T.; Chen, Y.-Z.; Chueh, Y.-L.; He, J.-H.; Chou, M.-Y.; Li, L.-J. Ultrahigh-Gain Photodetectors Based on Atomically Thin Graphene-MoS_2 Heterostructures. *Sci. Rep.* **2014**, *4*, 3826.

(11) Chen, C.; Feng, Z.; Feng, Y.; Yue, Y.; Qin, C.; Zhang, D.; Feng, W. Large-Scale Synthesis of a Uniform Film of Bilayer MoS_2 on Graphene for 2D Heterostructure Phototransistors. *ACS Appl. Mater. Interfaces* **2016**, *8*, 19004−19011.

(12) Singh, K.; Kumar, S.; Agarwal, K.; Soni, K.; Ramana Gedela, V.; Ghosh, K. Three-dimensional Graphene with MoS_2 Nanohybrid as Potential Energy Storage/Transfer Device. *Sci. Rep.* **2017**, *7*, 9458.

(13) Li, S.; Liu, Y.; Zhao, X.; Shen, Q.; Zhao, W.; Tan, Q.; Zhang, N.; Li, P.; Jiao, L.; Qu, X. Sandwich-Like Heterostructures of MoS_2/Graphene with Enlarged Interlayer Spacing and Enhanced Hydrophilicity as High-Performance Cathodes for Aqueous Zinc-Ion Batteries. *Adv. Mater.* **2021**, *33*, No. 2007480.

(14) Yu, J.; Yang, X.; Gao, G.; Xiong, Y.; Wang, Y.; Han, J.; Chen, Y.; Zhang, H.; Sun, Q.; Wang, Z. L. Bioinspired mechano-photonic artificial synapse based on graphene/MoS_2 heterostructure. *Sci. Adv.* **2021**, *7*, No. eabd9117.

(15) Cho, B.; Yoon, J.; Lim, S. K.; Kim, A. R.; Kim, D.-H.; Park, S.-G.; Kwon, J.-D.; Lee, Y.-J.; Lee, K.-H.; Lee, B. H.; Ko, H. C.; Hahm, M. G. Chemical Sensing of 2D Graphene/MoS_2 Heterostructure device. *ACS Appl. Mater. Interfaces* **2015**, *7*, 16775−16780.

(16) Tabata, H.; Sato, Y.; Oi, K.; Kubo, O.; Katayama, M. Bias- and Gate-Tunable Gas Sensor Response Originating from Modulation in the Schottky Barrier Height of a Graphene/MoS_2 van der Waals Heterojunction. *ACS Appl. Mater. Interfaces* **2018**, *10*, 38387−38393.

(17) Maitra, U.; Gupta, U.; De, M.; Datta, R.; Govindaraj, A.; Rao, C. N. R. Highly Effective Visible-Light-Induced H_2 Generation by Single-Layer 1T-MoS_2 and a Nanocomposite of Few-Layer 2H-MoS_2 with Heavily Nitrogenated Graphene. *Angew. Chem., Int. Ed.* **2013**, *52*, 13057−13061.

(18) Liu, Y.; Huang, Y.; Duan, X. Van der Waals integration before and beyond two-dimensional materials. *Nature* **2019**, *567*, 323−333.

(19) Liu, Y.; Weiss, N. O.; Duan, X.; Cheng, H.-C.; Huang, Y.; Duan, X. Van der Waals heterostructures and devices. *Nat. Rev. Mater.* **2016**, *1*, 16042.

(20) Kretinin, A. V.; Cao, Y.; Tu, J. S.; Yu, G. L.; Jalil, R.; Novoselov, K. S.; Haigh, S. J.; Gholinia, A.; Mishchenko, A.; Lozada, M.; Georgiou, T.; Woods, C. R.; Withers, F.; Blake, P.; Eda, G.; Wirsig, A.; Hucho, C.; Watanabe, K.; Taniguchi, T.; Geim, A. K.; Gorbachev, R. V. Electronic Properties of Graphene Encapsulated with Different Two-Dimensional Atomic Crystals. *Nano Lett.* **2014**, *14*, 3270−3276.

(21) Pramoda, K.; Gupta, U.; Ahmad, I.; Kumar, R.; Rao, C. N. R. Assemblies of covalently cross-linked nanosheets of MoS_2 and of MoS_2−RGO: synthesis and novel properties. *J. Mater. Chem. A* **2016**, *4*, 8989−8994.

(22) Pramoda, K.; Ayyub, M. M.; Singh, N. K.; Chhetri, M.; Gupta, U.; Soni, A.; Rao, C. N. R. Covalently Bonded MoS_2−Borocarbonitride Nanocomposites Generated by Using Surface Functionalities on the Nanosheets and Their Remarkable HER Activity. *J. Phys. Chem. C* **2018**, *122*, 13376−13384.

(23) Chen, X.; Kohring, M.; Assebban, M.; Tywoniuk, B.; Bartlam, C.; Moses Badlyan, N.; Maultzsch, J.; Duesberg, G. S.; Weber, H. B.; Knirsch, K. C.; Hirsch, A. Covalent Patterning of 2D MoS_2. *Chem. − Eur. J.* **2021**, *27*, 13117−13122.

(24) Matsuura, T.; Omura, K. Photo-induced Reactions. III. The Synthesis of Biphenyls from Aromatic Bromo-Compounds. *Bull. Chem. Soc. Jpn.* **1966**, *39*, 944−947.

(25) Hirsch, A.; Hauke, F. Post-Graphene 2D Chemistry: The Emerging Field of Molybdenum Disulfide and Black Phosphorus Functionalization. *Angew. Chem., Int. Ed.* **2018**, *57*, 4338−4354.

(26) Bottari, G.; Herranz, M. Á.; Wibmer, L.; Volland, M.; Rodríguez-Pérez, L.; Guldi, D. M.; Hirsch, A.; Martín, N.; D'Souza,

F.; Torres, T. Chemical functionalization and characterization of graphene-based materials. *Chem. Soc. Rev.* **2017**, *46*, 4464−4500.
(27) Vecera, P.; Chacón-Torres, J. C.; Pichler, T.; Reich, S.; Soni, H. R.; Görling, A.; Edelthalhammer, K.; Peterlik, H.; Hauke, F.; Hirsch, A. Precise determination of graphene functionalization by in situ Raman spectroscopy. *Nat. Commun.* **2017**, *8*, 15192.
(28) Bertolazzi, S.; Gobbi, M.; Zhao, Y.; Backes, C.; Samorì, P. Molecular chemistry approaches for tuning the properties of two-dimensional transition metal dichalcogenides. *Chem. Soc. Rev.* **2018**, *47*, 6845−6888.
(29) Mignuzzi, S.; Pollard, A. J.; Bonini, N.; Brennan, B.; Gilmore, I. S.; Pimenta, M. A.; Richards, D.; Roy, D. Effect of disorder on Raman scattering of single-layer MoS_2. *Phys. Rev. B* **2015**, *91*, No. 195411.
(30) Chen, X.; Bartlam, C.; Lloret, V.; Moses Badlyan, N.; Wolff, S.; Gillen, R.; Stimpel-Lindner, T.; Maultzsch, J.; Duesberg, G. S.; Knirsch, K. C.; Hirsch, A. Covalent Bisfunctionalization of Two-Dimensional Molybdenum Disulfide. *Angew. Chem., Int. Ed.* **2021**, *60*, 13484−13492.
(31) Almadori, Y.; Bendiab, N.; Grévin, B. Multimodal Kelvin Probe Force Microscopy Investigations of a Photovoltaic WSe_2/MoS_2 Type-II Interface. *ACS Appl. Mater. Interfaces* **2018**, *10*, 1363−1373.
(32) Tosun, M.; Fu, D.; Desai, S. B.; Ko, C.; Seuk Kang, J.; Lien, D.-H.; Najmzadeh, M.; Tongay, S.; Wu, J.; Javey, A. MoS_2 Heterojunctions by Thickness Modulation. *Sci. Rep.* **2015**, *5*, 10990.
(33) van Druenen, M.; Collins, G.; Glynn, C.; O'Dwyer, C.; Holmes, J. D. Functionalization of SiO2 Surfaces for Si Monolayer Doping with Minimal Carbon Contamination. *ACS Appl. Mater. Interfaces* **2018**, *10*, 2191−2201.

https://doi.org/10.1021/jacs.2c00642
J. Am. Chem. Soc. 2022, 144, 9645−9650